Article

High-Pressure Hydrogenation: A Path to Efficient Methane Production from CO$_2$

Maitê L. Gothe [1] , **Adolfo L. Figueredo** [1] , **Laís R. Borges** [1] , **Ruben Ramos** [2] , **Andreia F. Peixoto** [3]
and **Pedro Vidinha** [1,*]

1   Instituto de Química, Universidade de São Paulo, Av. Prof. Lineu Prestes 748, Butantã 05508-900, São Paulo, Brazil; maite.gothe@usp.br (M.L.G.); adolfofigueredo@usp.br (A.L.F.); laisreisborges@usp.br (L.R.B.)
2   Iberian Centre for Research in Energy Storage (CIIAE), 10004 Cáceres, Extremadura, Spain; rrvelarde@hotmail.com
3   LAQV-REQUIMTE, Departamento de Química e Bioquímica, Faculdade de Ciências, Universidade do Porto, Rua do Campo Alegre s/n, 4169-007 Porto, Portugal; andreia.peixoto@fc.up.pt
*   Correspondence: pvidinha@iq.usp.br

Abstract: Methane has a rather relevant role in the "Power-to-Gas" concept, which is central in the current paradigm of climate change and renewable energies. Methane, the main component of natural gas, can be produced by catalytic hydrogenation reactions, particularly of CO$_2$. A very effective catalyst in this reaction, hydrotalcite-derived nickel nanoparticles supported on alumina, Ni/Al$_2$O$_3$-HTC, can be employed in a high-pressure flow reactor to convert CO$_2$ and H$_2$ into CH$_4$ at 100% selectivity and 84% conversion, whereas at atmospheric pressure, methane can be obtained with up to 90% selectivity. The high-pressure aspect also allows fast-paced production—over 5 m$^3 \cdot$h$^{-1} \cdot$kg$_{cat}$$^{-1}$ of CH$_4$ can be generated.

Keywords: methanation; Power-to-Gas; catalysis; CO$_2$ conversion; hydrotalcite

1. Introduction

The recent shifts in geopolitics have had a profound impact on energy transition policies. Natural gas has, for many, been seen as a gradual path toward decarbonization. However, recent developments, especially in Europe, have led to an increase in natural gas prices and the exploration of alternative energy sources to meet current demands [1]. In this context, hydrogen has emerged as an attractive option to fuel the European economy, with numerous projects for its production underway across Europe [2]. However, hydrogen faces challenges such as low power density and storage difficulties, which hinder its widespread adoption. Nonetheless, hydrogen can be readily converted into other products that can seamlessly integrate into existing energy pipelines. The production of synthetic methane is one of the valuable outcomes achievable through the hydrogenation of CO$_2$ [3]. This process not only facilitates the global utilization of hydrogen but also plays a crucial role in decarbonization efforts. This is because the CO$_2$ used in the production of synthetic methane can originate from specific industrial processes, thereby becoming part of a sustainable cycle that ultimately reduces carbon emissions [4].

Therefore, CO$_2$ methanation is relevant in the context of carbon utilization and sustainable energy and it fits into the "Power-to-Gas" concept as a way to store energy produced by intermittent renewable sources such as solar or wind [5]. The hydrogenation of CO$_2$ to CH$_4$ over nickel-based catalysts is particularly effective and is currently employed at industrial scale, since it has a good combination of the low cost of non-noble metals and high catalytic activity [6–9]. Particularly, catalysts of the composition Ni/Al$_2$O$_3$ are often studied for this reaction [10,11]. The catalytic activity of Ni/Al$_2$O$_3$ is rather sensitive to the synthesis methodology [12]. Ni/Al$_2$O$_3$ synthesized from hydrotalcite (HTC) has been demonstrated to be a distinctly active catalyst for the CO$_2$ methanation reaction. Ni/Al$_2$O$_3$-HTC has been

shown to contain more basic active sites, which leads to a higher CO_2 conversion when compared with Ni/Al_2O_3 synthesized by the wet impregnation method [13]. Additionally, the strong metal-support interaction present in hydrotalcite-derived catalysts leads to an intrinsically high dispersion of the metal on the support, even at high loadings, which helps prevent sintering and catalyst deactivation [14].

The CO_2 methanation reaction has a complex relationship with temperature. On the one hand, the thermodynamic equilibrium of this reaction indicates that low temperatures favor higher CO_2 conversion and selectivity to CH_4, but the kinetic barriers demand higher temperatures to be overcome [15]. High pressure could be a powerful tool to increase the methane yield and avoid carbon deposition. In a thermodynamic equilibrium analysis of the CO_2 methanation, Jürgensen et al. found that at increased pressures, carbon deposition can be inhibited, which could delay catalyst deactivation [16]. Mutz et al. also verified experimentally that increasing pressure from 1 to 10 bar improved CO_2 conversion and methane selectivity [17]. Here, an efficient process for the hydrogenation of CO_2 to CH_4 over hydrotalcite-derived Ni/Al_2O_3 is evaluated over a broad range of temperatures (200–800 °C) and pressures (1–80 bar). The demonstration of the positive effect of high pressure on the conversion and selectivity of the CO_2 methanation process is a highlighted topic in this work. Likewise, the stability and reusability of the catalyst is evaluated through the characterization of spent samples with the objective of establishing a consistent understanding of the design of heterogeneous catalysts for the competitive production of synthetic methane from CO_2 emissions.

2. Results

The hydrotalcite-derived Ni/Al_2O_3-HTC catalyst contained 15 wt% Al and 43 wt% Ni, as revealed by ICP-OES elemental analysis, which is in agreement with the theoretical molar ratio. The BET surface area of the as-prepared catalyst was found to be 175 $m^2 \cdot g^{-1}$, with a pore volume of 0.50 $cm^3 \cdot g^{-1}$ and pore radius of 2 nm. After thermal treatment under H_2 at 500 °C for 1 h, the BET surface area increased to 247 $m^2 \cdot g^{-1}$, the pore volume increased to 0.57 $cm^3 \cdot g^{-1}$ and the pore radius increased to 2.7 nm. The pore size distributions were measured with the BJH method over the adsorption isotherm. The N_2 adsorption-desorption isotherms can be found in the Supplementary Materials, along with the graphs of BJH pore-size distributions (Figures S1–S4). This difference in surface area may be related to changes in the proportion of amorphous $NiAl_2O_4$ or Al_2O_3 and metallic Ni, which is caused by the reduction process and leads to different morphologies [18].

The temperature-programmed reduction of the hydrotalcite-derived Ni/Al_2O_3-HTC catalyst can be found in Figure 1a. A small and broad peak of hydrogen consumption is present around 250 °C, which can be attributed to the reduction of NiO species with low interaction with the Al_2O_3 support, and a sharp increase in H_2 consumption starts around 500 °C and with a maximum at 558 °C, which may be due to the reduction of a different species of Ni of stronger interaction with the Al_2O_3 support. Similar TPR results have been reported for another Ni/Al_2O_3 catalyst by Xu et al. [19]. Since H_2 consumption starts to increase at 500 °C, this was the temperature chosen for the pre-reduction step performed prior to reaction.

The XRD of the as-prepared and reduced catalysts (Figure 1b) showed no sign of Al_2O_3, which indicates that the alumina support is amorphous. The catalyst as prepared contained peaks matched to NiO (ICSD 76959) at 37.6°, 43.7°, 63.6°, 76.3°, and 80.4°. The average crystallite size of NiO phases on the catalyst as prepared was 3.9 nm. When the catalyst was reduced at 500 °C under H_2, the XRD peaks matched metallic Ni (ICSD 52265) at 44.5°, 51.9°, and 76.5°, with an average crystallite size of metallic Ni of 7.6 nm, although some broadened and low intensity peaks related to NiO were still visible, which suggests nickel was not fully reduced. These crystallite sizes are smaller than reported for Ni/Al_2O_3 catalysts of similar Ni weight content but synthesized from γ-Al_2O_3—i.e., Hu et al. found a 14.1 nm crystallite size for a Ni/γ-Al_2O_3 catalyst of 40 wt% Ni [11], which emphasizes the effect of the hydrotalcite precursor [11]. The average crystallite size of the Ni particles

was estimated through Rietveld refinement of the XRD analyses for the reduced and spent catalysts, performed with Profex software version 5 [20]. The parameters obtained for the Rietveld refinement can be found in Table 1. Transmission electronic microscopy (TEM) images of the reduced catalyst were also used to obtain a size distribution of Ni nanoparticles (Figure 2). An average size of 8.7 ± 2.7 nm was found, which is similar to the crystallite size calculated from XRD.
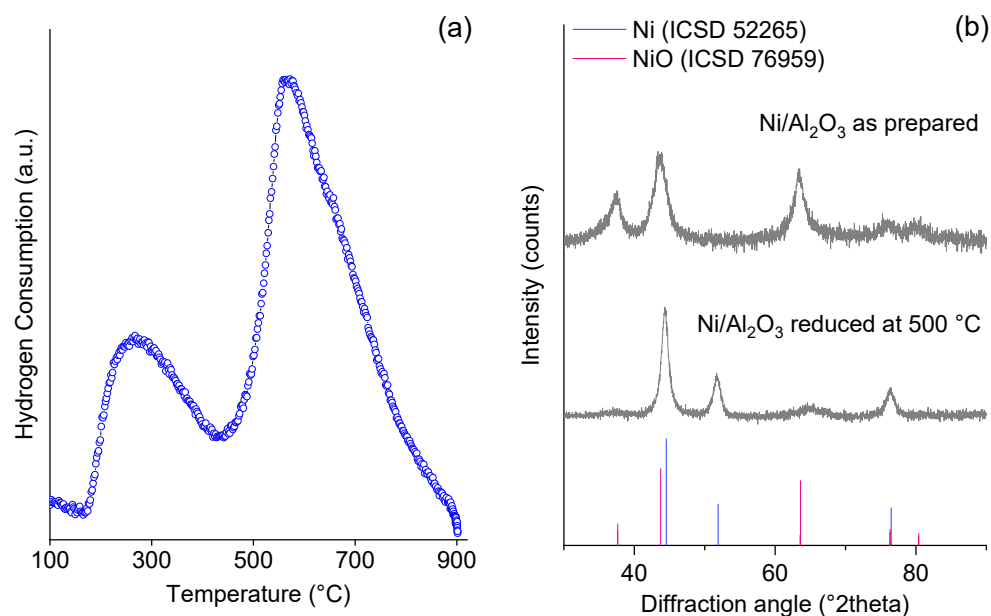

Figure 1. (**a**) Temperature-programmed reduction (TPR) of as-prepared Ni/Al$_2$O$_3$-HTC; (**b**) XRD pattern of the Ni/Al$_2$O$_3$ catalyst as prepared and reduced at 500 °C.
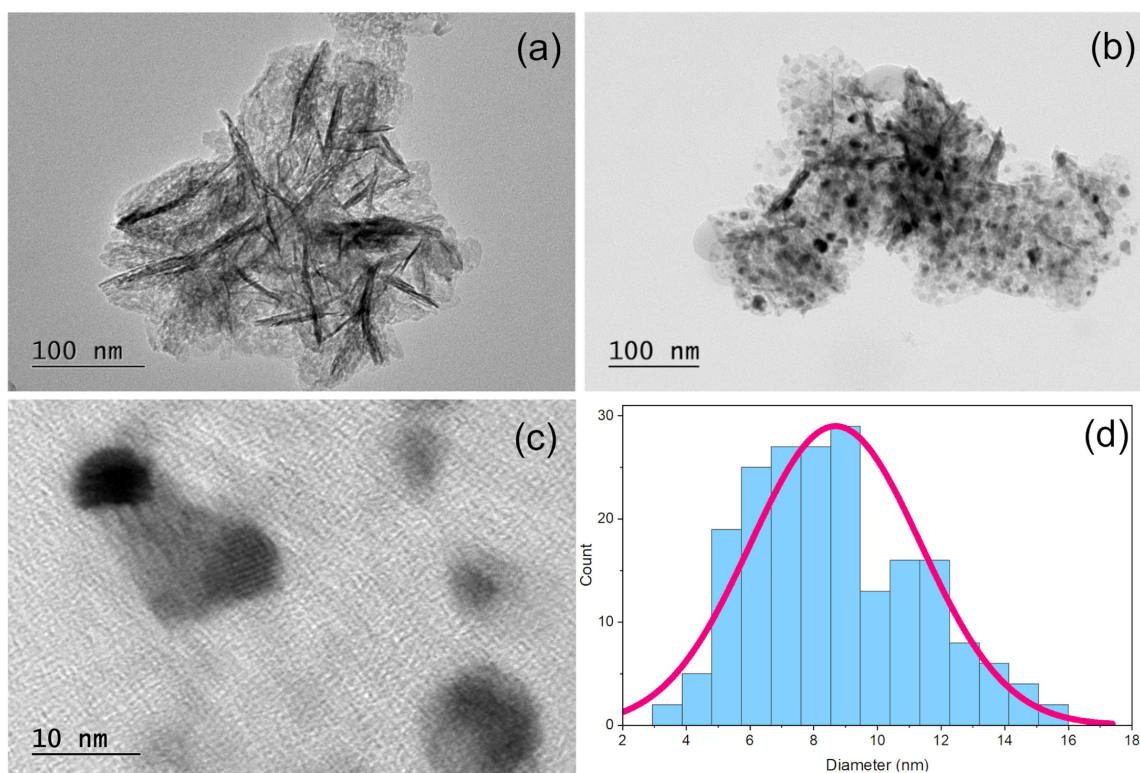

Figure 2. Transmission electronic microscopy (TEM) images of Ni/Al$_2$O$_3$-HTC (**a**) as-prepared; (**b**,**c**) reduced at 500 °C under H$_2$; (**d**) histogram size distribution of Ni nanoparticles.

Table 1. Rietveld refinement statistics performed on the XRD of the Ni/Al$_2$O$_3$-HTC catalyst.

Ni/Al$_2$O$_3$-HTC	As Prepared	Reduced	Spent
Crystallite size/nm	3.9	7.6	42.4
Rp	1.7%	1.7%	0.5%
X^2	1.13	1.22	<0.01
NiO	1.00	0.02	0.01
Ni metal	-	0.98	0.99

The activity of the CO_2 methanation reaction under atmospheric pressure over Ni/Al$_2$O$_3$-HTC, seen in Figure 3, produces CH_4 and CO as the side product. The selectivity to CH_4, calculated as mols of CH_4 divided by mols of converted CO_2, reached its maximum value of 90% around 450 °C, at which point the CO_2 conversion rate was of 37%. The CO_2 conversion rate maximized at 79% at the highest temperature studied, 800 °C, but at this point the selectivity to CH_4 was close to zero and the reaction yielded mostly CO. The high selectivity to methane at low temperatures was expected since it is an exothermic reaction. The rate of methane production, shown in Figure 3b, was calculated based on the initial flow of CO_2, the conversion, and methane selectivity. The maximum methane production at atmospheric pressure, obtained at 487 °C, was of 0.12 $mol_{CH4} \cdot g_{cat}^{-1} \cdot h^{-1}$, which corresponds to 2.7 $L_{CH4} \cdot g_{cat}^{-1} \cdot h^{-1}$, and a 45% yield.
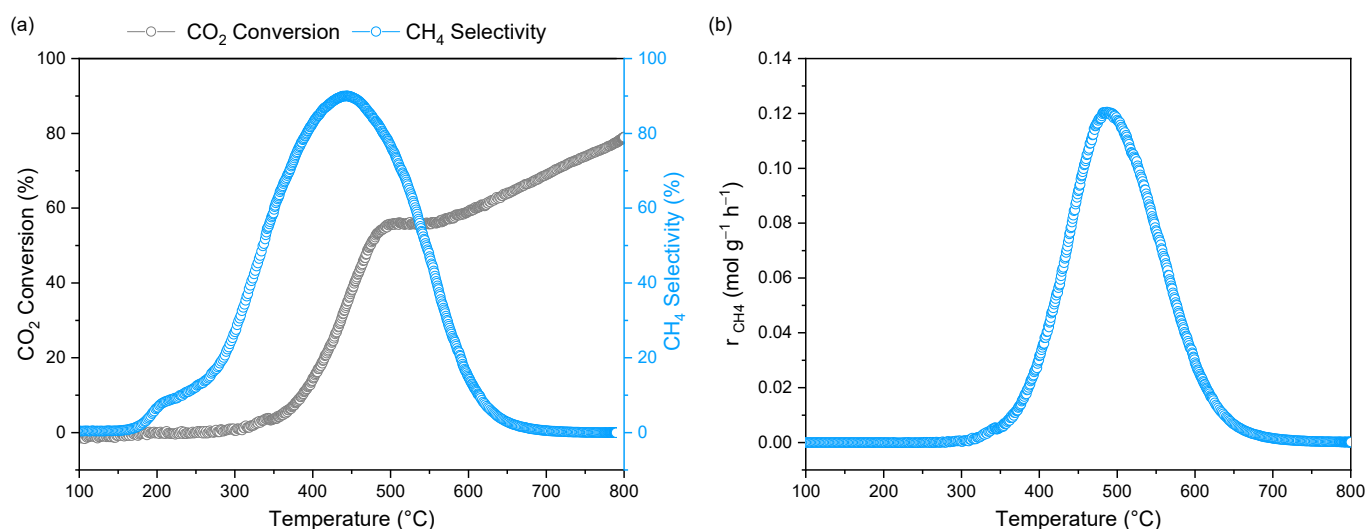

Figure 3. Effect of temperature on CO_2 hydrogenation at atmospheric pressure over Ni/Al$_2$O$_3$-HTC. Reaction conditions: Ni/Al$_2$O$_3$-HTC pre-reduced at 500 °C, atmospheric pressure, CO_2:H_2 = 1:4, GHSV = 30,000 $mL \cdot g_{cat}^{-1} \cdot h^{-1}$. (**a**) CO_2 conversion and CH_4 selectivity; (**b**) CH_4 production rate.

The performance of the high-pressure CO_2 methanation is shown in Figure 4. A positive correlation between pressure and CO_2 hydrogenation to methane is observed, as expected due to the thermodynamic equilibrium of this reaction (Figure 4a). The selectivity to CH_4 was 100% in all high-pressure conditions tested, which means CO_2 conversion equals CH_4 yield. The high-pressure process also allows for a large quantity of reactants to be processed at a given time rate. For instance, in this process, at the optimal conditions of 450 °C and 80 bar, with a selectivity of 100% and conversion of 84%, given the space velocity of 30,000 $mL \cdot g_{cat}^{-1} \cdot h^{-1}$ with a CO_2:H_2 ratio of 1:4, 6 $L \cdot g_{cat} h^{-1}$ of CO_2 can be processed and yield 5.04 $L \cdot g_{cat} h^{-1}$ of CH_4. In an extrapolation to a potential scale up, 5.04 cubic meters of CH_4 could be produced per kilogram of catalyst per hour.
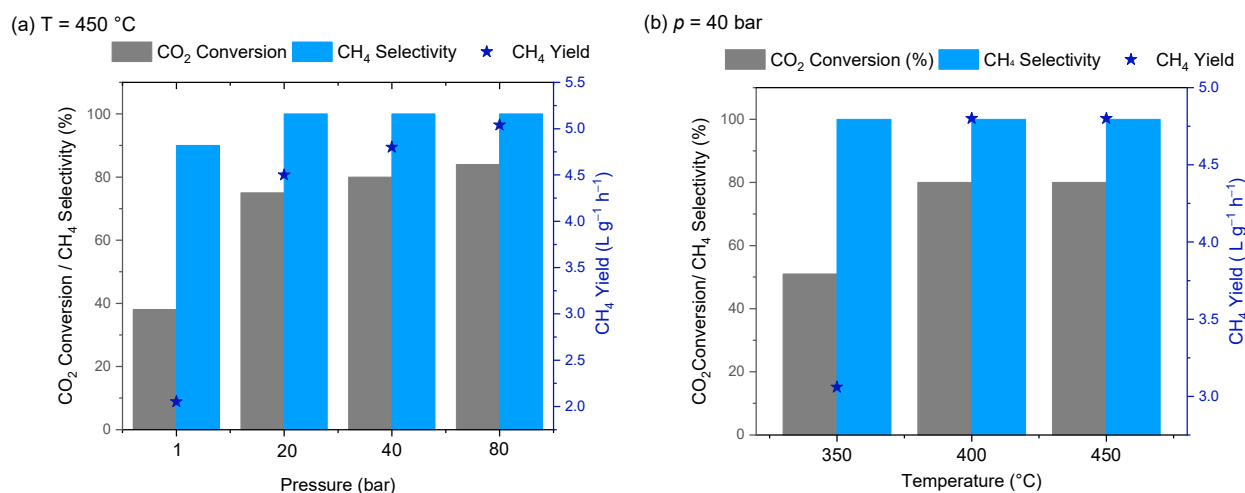
(a) T = 450 °C

(b) *p* = 40 bar

Figure 4. (**a**) Effect of pressure at 450 °C and (**b**) effect of temperature at 40 bar on CO_2 methanation over Ni/Al_2O_3-HTC. Reaction conditions: fixed-bed reactor packed 200 mg of Ni/Al_2O_3 pre-reduced at 500 °C, CO_2:H_2 = 1:4, GHSV = 30,000 mL·g_{cat}^{-1}·h^{-1}.

In terms of methane space time yield (STY), at 450 °C the production rate of CH_4 increased from 2.05 L_{CH4}·g_{cat}^{-1}·h^{-1} at atmospheric pressure to 4.50 and 4.80 L_{CH4}·g_{cat}^{-1}·h^{-1} when the pressure was elevated from 1 to 20 bar and 40 respectively. A maximum of methane yield was achieved at 80 bar and 450 °C, with a STY of 5.04 L_{CH4}·g_{cat}^{-1}·h^{-1}. This is an increase in methane STY of 2.5 times when the pressure increased from 1 to 80 bar.

The effect of reaction temperature on the high-pressure methanation of CO_2 can be viewed in Figure 4b. The hydrogenation of CO_2 to CH_4 is an exothermic reaction, and is therefore thermodynamically hindered by higher temperatures [6]. Despite this thermodynamic effect, the increase in temperature from 350 °C to 450 °C was observed to be beneficial for the conversion of CO_2 to CH_4, since it helps the CO_2 gas phase reaction to overcome its kinetic limitations. Moreover, at high pressure, the negative effect of temperature increases on the thermodynamic equilibrium of CO_2 methanation is less pronounced [15]. At the lower reaction temperature of 350 °C and high pressure of 40 bar, a CO_2 conversion of 51% was obtained with 100% selectivity to CH_4, whereas at atmospheric pressure and the same temperature of 350 °C, a CO_2 conversion of only 4% was observed with a 58% selectivity to CH_4.

The reaction over Ni/Al_2O_3-HTC was 100% selective to methane over the range of temperatures and high pressures tested, with no formation of CO through the reverse water-gas shift reaction and no other hydrocarbon or alcohol observed. The absence of CO and maximized CH_4 selectivity in the high-pressure reactions is related to a thermodynamic effect. As seen in Equations (1) and (2), CO_2 hydrogenation to CH_4 occurs with a volume contraction, unlike CO_2 hydrogenation to CO. Therefore, high pressure is remarkably favorable for CO_2 methanation, since it shifts the equilibrium towards the volume contraction.

$$CO_2 + 4\,H_2 \rightleftharpoons CH_4 + 2\,H_2O \qquad (1)$$

$$CO_2 + H_2 \rightleftharpoons CO + H_2O \qquad (2)$$

The methane yield of the high-pressure CO_2 methanation catalyzed by Ni/Al_2O_3-HTC at 40 bar was 51% at 350 °C and increased to 80% at 400 °C, with no significant changes at 450 °C. Therefore, the high pressure allows the CO_2 methanation reaction to maintain high yields at higher temperatures, which is advantageous since this is an exothermic reaction and temperature control can be an issue when reactor hot spots lead to decreased activity [14]. The CO_2 methanation reaction has been reported in the literature over a variety of Ni-based catalysts at atmospheric pressure, in which case the CH_4 yield starts to decrease

as temperatures increase [7,17,21]. Yi et al. reported a CO_2 conversion of around 60% for the temperature range of 350–450 °C at atmospheric pressure over a similar catalyst Ni/γ-Al_2O_3 of 45 wt% Ni and CH_4 selectivity of 95% for the temperatures of 350–400 °C [21], noticing a decrease in selectivity to 80% when the temperature reached 450 °C. Kowalik et al. found a CO_2 conversion of 40% for these conditions over Ni/α-Al_2O_3, in which case the CH_4 selectivity also decreased at temperatures higher than 400 °C [22]. These similar findings reinforce that, at ambient pressure, even with effective catalysts, the selectivity to CH_4 is hindered at higher temperatures.

As seen in Table 2, CHN elemental analyses performed on the $NiAl_2O_3$-HTC catalyst as prepared and spent after 6 h of reaction at 400 °C reveal that the carbon content did not significantly change after the reaction, indicating that carbon deposition would not be an issue either under 40 bar of pressure or atmospheric pressure. In addition, a time-on-stream plot of the reaction at 400 °C and 40 bar (Figure S7 in Supplementary Materials) showed that the reaction was stable for 7 h at 80% CO_2 conversion and 100% CH_4 selectivity.

Table 2. CHN elemental analyses of Ni/Al_2O_3-HTC catalyst as prepared and spent at high pressure or at ambient pressure.

Sample	%C	%H	%N
Ni/Al_2O_3-HTC as prepared	0.44 ± 0.04	1.29 ± 0.04	0.02 ± 0.01
Ni/Al_2O_3-HTC spent (40 bar)	0.40 ± 0.06	0.24 ± 0.06	0.04 ± 0.04
Ni/Al_2O_3-HTC spent (1 bar)	0.40 ± 0.06	0.59 ± 0.08	-

Ni 2p XPS analyses were used to explore the surface composition of the Ni/Al_2O_3 catalyst as prepared, reduced, and spent after CO_2 methanation at 40 bar and 400 °C (Figure 5 and Table 3). A Shirley baseline was applied to all spectra. Ni 2p components were fitted with a GL(30) line shape. The BE difference due to spin orbit coupling of Ni 2p was fitted as 17.27 eV for Ni^0, 17.8 eV for NiO, and 17.6 eV for $NiAl_2O_4$. The surface of the as-prepared catalyst contained 74 At% of $NiAl_2O_4$, interpreted as the peak of binding energy (BE)~856.04 eV, and 26% of NiO, at 853.84 eV. It is noteworthy that the XRD of the as-prepared Ni/Al_2O_3 catalyst (Figure 1b) only revealed the diffraction pattern of NiO, which suggests that the $NiAl_2O_4$ phase observed by XPS was amorphous, as the originate Al_2O_3 was also amorphous. This composition was expected from a hydrotalcite-derived nickel-alumina catalyst and is in line with previous reports [21–26].

When reduced at 500 °C under H_2 for 1 h, the surface of the Ni/Al_2O_3-HTC catalyst presented a metallic Ni peak of ~852.00 eV, which accounts for 31 At% of nickel contribution on the surface. The increase in metallic Ni surface At% observed after reduction of the catalyst was accompanied by a decrease of $NiAl_2O_4$ to 37 At%. NiO was also present on the surface of the reduced catalyst at 32 At%. The spent catalyst, in turn, presented a much lower At% of metallic Ni of only 1%, and increased NiO At% of 54, which could be explained by oxidation during reaction; however, a more probable cause was the oxidation due to prolonged exposition to air previous to XPS analysis, as the XPS analysis was performed ex situ. The Al 2p region of the XPS of the Ni/Al_2O_3-HTC catalyst showed peaks of Al 2p at 74.8, 75.6, and 74.8 eV for the catalyst as prepared, reduced, and spent, respectively. These energies are coherent with a Al_2O_3 species [27]. The slight shift to lower energy observed in the as-prepared sample could be linked to a stronger interaction of Al_2O_3 with oxidized Ni as a $NiAl_2O_4$ species. On the other hand, the reduced catalyst presented a weakened interaction of metallic Ni with the Al_2O_3 support, therefore the energy of the Al 2p orbital in the reduced catalyst closely matched the energy reported for pure Al_2O_3 at 75.6 eV [27]. The XPS in the O 1s region of these samples can be found in SI (Figure S5) and corroborates these conclusions.
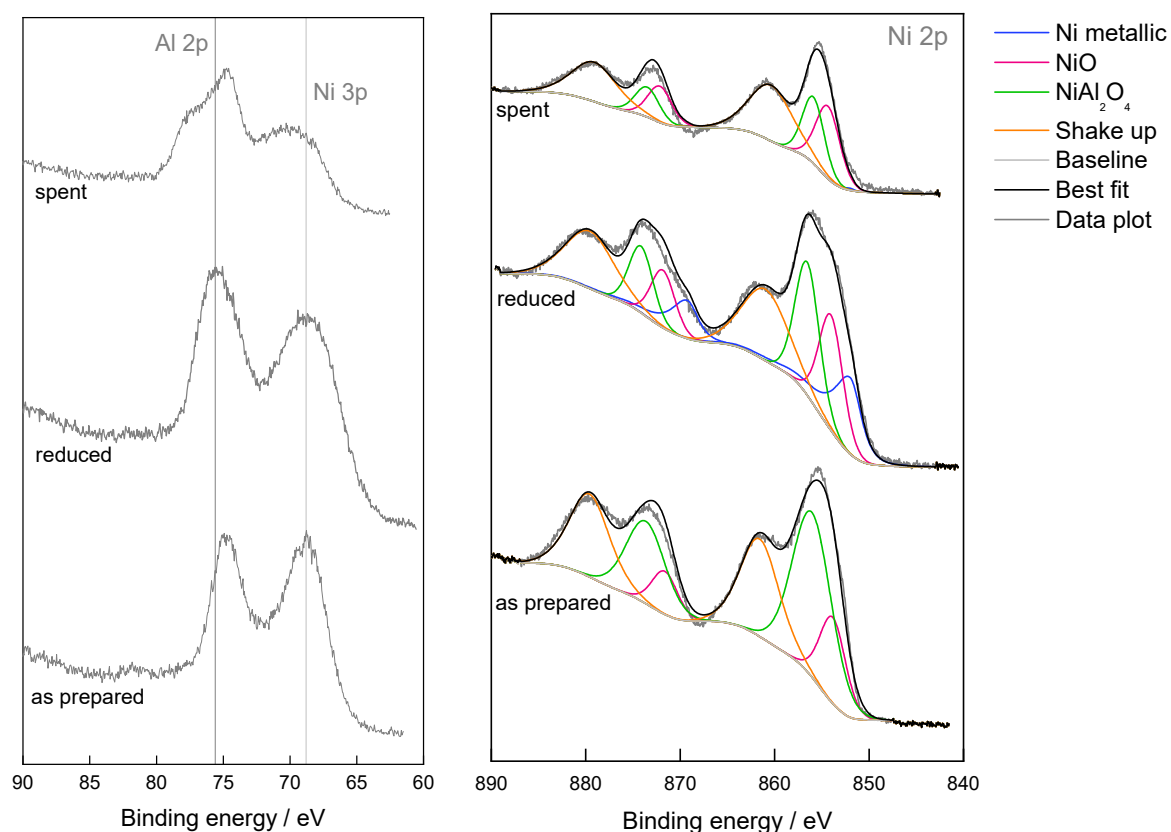
Figure 5. Al 2p and Ni 2p XPS of Ni/Al$_2$O$_3$-HTC catalyst as prepared, reduced, and spent after CO$_2$ hydrogenation at 400 °C and 40 bar. 30 scans collected at E$_{pass}$ = 20 eV and 0.05 eV step.

Table 3. Surface composition of the Ni/Al$_2$O$_3$-HTC catalyst obtained from Ni 2p XPS data.

Ni/Al$_2$O$_3$-HTC	%At of Surface Elements			%At of Surface Ni Species		
	Ni	Al	O	Ni Metallic	NiO	NiAl$_2$O$_4$
As prepared	21	36	43	-	26	74
Reduced	13	36	50	31	32	37
Spent	11	33	56	1	54	45

The XRD of the spent catalyst (Figure 6a) shows well-defined peaks attributed to metallic Ni, whereas the XPS indicates that the surface of the catalyst after reaction was composed mostly of NiO. This discrepancy in XRD and XPS data indicates that the bulk structures of both the reduced and the spent catalyst were mostly metallic nanoparticles, even if their surfaces may have contained NiO. Although metallic Ni is essential for H$_2$ activation, this residual content of NiO on the catalytic surface may play a role in the reactivity of this material. Residual NiO has been suggested to hinder the agglomeration of metallic Ni nanoparticles [28]. Moreover, the presence of NiO can facilitate the activation of CO$_2$ and the hydrogenation of oxygenated and CO intermediates to CH$_4$ on a metal/oxide interface, as previously reported for similar materials [29–31]. As seen in Table 1, the nickel nanoparticles on the catalyst Ni/Al$_2$O$_3$-HTC appeared to grow from 7.6 nm to 42.4 nm after exposure to the CO$_2$ hydrogenation reaction conditions, which is a considerable increase in size, although they still maintained their nanometric dimensions.
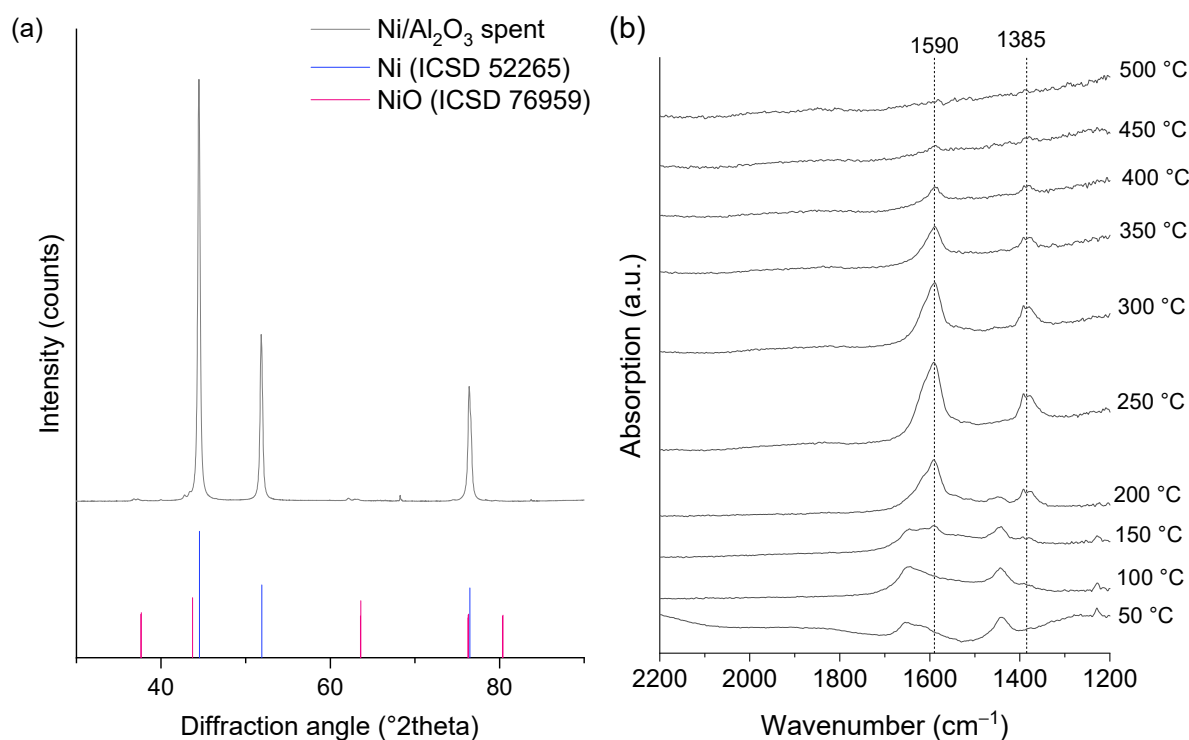
Figure 6. (**a**) XRD pattern of the Ni/Al$_2$O$_3$-HTC catalyst spent after CO$_2$ hydrogenation to CH$_4$ at 400 °C and 40 bar; (**b**) DRIFTS of CO$_2$ methanation reaction over Ni/Al$_2$O$_3$-HTC pre-reduced at 500 °C at different temperatures, atmospheric pressure, and CO$_2$:H$_2$ = 1:4. All spectra were baseline-corrected with spectra recorder under Ar at the same temperature.

A CO$_2$-TPD profile of Ni/Al$_2$O$_3$-HTC pre-reduced at 500 °C (Figure S6) revealed a peak of CO$_2$ desorption at 127 °C, which indicates that this catalyst has basic sites of weak interaction with CO$_2$. The CO$_2$ desorption peak at temperatures between 100–150 °C may be attributed to the interaction of CO$_2$ with surface hydroxyls, and is often found in nickel-hydrotalcite materials [32,33]. The presence of surface hydroxyls on Ni materials has also been linked to their catalytic activity in CO$_2$ methanation, as CO$_2$ adsorbed on -OH groups facilitates the formation of reactive carbonate species, which, under reaction conditions, are hydrogenated to formate, and subsequently to methane [34]. In order to shed light on the reaction intermediates that may be adsorbed on the catalytic surface and help explain the high CH$_4$ selectivity obtained, diffuse reflectance infrared Fourier-transform spectroscopy (DRIFTS) analysis of the CO$_2$ methanation reaction over the catalyst Ni/Al$_2$O$_3$-HTC was performed over a range of reaction temperatures, as seen in Figure 6b. At the lower temperatures of 50–100 °C, the bands seen around 1650 cm^{-1} and 1445 cm^{-1} can be denoted as adsorbed carbonate species [35]. Bands around 1590 cm^{-1} and 1385 cm^{-1} can be attributed to formate species adsorbed on the surface of the Ni/Al$_2$O$_3$-HTC catalyst [35]. These adsorbed formate species appeared at 200 °C and grew in intensity up to 300 °C, then started to desorb at 350 °C and could no longer be detected at 500 °C. As observed by CO$_2$ hydrogenation at atmospheric pressure (Figure 3a), for temperatures higher than 400 °C, the CO$_2$ conversion was higher than 20%, which can explain the lack of adsorbed formate species on the DRIFTS experiment, since at high conversion, the species adsorb and desorb quickly. No bands are observed in the 2000–2100 cm^{-1} range, which indicates the absence of adsorbed CO. These findings may suggest that the reaction mechanism of the methanation of CO$_2$ over Ni/Al$_2$O$_3$-HTC occurred via a formate pathway, which is in agreement with the literature on similar catalysts [11,35]. In this mechanistic route, CO$_2$ adsorbed on the catalytic surface was hydrogenated to adsorbed formate species, which were observed by DRIFTS, then subsequently hydrogenated and desorbed as the final product methane.

3. Materials and Methods

The hydrotalcite-derived Ni/Al$_2$O$_3$-HTC catalyst was synthesized according to a method previously described by Ramos et al. [32]. Briefly, 1.5 M aqueous solutions of AlCl$_3$·H$_2$O and NiCl$_2$·H$_2$O were added to an aqueous solution of urea. The mixture was refluxed at 95 °C under stirring, aged for 65 h, and filtered. The precipitate was suspended in a solution of NH$_4$HCO$_3$ to remove residual Cl, washed with water and dried at 95 °C. Finally, the material was calcined at 500 °C in air for 5 h.

X-ray diffraction (XRD) patterns of the catalysts were obtained with a Rigaku Miniflex diffractometer using Cu Kα radiation, 40 kV tension, and 30 mA current, with a step of 2θ of 0.02° at 2°/min. Elemental percentages of Ni and Al on the Ni/Al$_2$O$_3$-HTC catalysts were evaluated by Inductively Coupled Plasma Optical Emission Spectrometry (ICP-OES) in a Spectro Arcos spectrometer. Samples were previously digested by alkaline fusion with lithium tetraborate at 980 °C and then dissolved in nitric acid. Elemental percentages of CHN were obtained from a Perkin Elmer 2400 series ii elemental analyzer. X-ray photoelectron spectroscopy (XPS) data were obtained with a Specs instrument with monochromatic Al Kα of excitation energy = 1486.71 eV. A constant pass energy of 20 eV and a step of 0.05 eV were applied on all high-resolution spectra. CasaXPS software version 2.3.25 was used for peak fitting, and the C 1 s peak on adventitious carbon was calibrated to 284.8 eV.

The atmospheric pressure hydrogenation of CO$_2$ was performed in a Hiden Analytical Catlab reactor connected to a mass spectrometer. A fixed bed reactor was packed with 50 mg of catalyst, the pre-reduction was carried out under a hydrogen flow at 500 °C, then the catalyst was cooled down to 100 °C under argon flow and fed with the reactants at 30,000 mL·g^{-1}·h^{-1} at a ratio of CO$_2$:H$_2$ equal to 1:4. For the high-pressure reactions, a fixed-bed flow reactor was packed with 200 mg of the as-prepared catalyst, which was pre-reduced in situ under pure H$_2$ under atmospheric pressure at 500 °C for 1 h before all reactions. The heating ramp employed was of 10 °C/min in all reactions and pre-reduction steps. A spring-loaded backpressure valve was used to maintain the reaction pressure at the desired value. The exit of the backpressure valve was connected to a GC System (Shimadzu GC-2030) comprised of two thermal conductivity detectors (TCD) and one flame ionization detector (FID) for analysis of the reaction mixture. The chromatographic columns used were Rt-Msieve 5A PLOT for the detection of CO and CH$_4$, Rt-Q-BOND PLOT for the detection of CO$_2$ and C$_2$, Rtx-1 for hydrocarbons and alcohols, and molecular sieve 5A for H$_2$. CO, CH$_4$, and CO$_2$ were quantified by TCD-1 with He as reference gas, while H$_2$ was quantified by TCD-2 with N$_2$ as reference, and other long chain hydrocarbons or alcohols formed would have been detected by FID. All columns were preceded by Porapak-N pre-columns. The calibration of the GC detectors was performed with a standard mixture cylinder sold by Messer. The reagents CO$_2$ and H$_2$ were fed into the reactor by a set of syringe pumps. All catalytic tests were performed in triplicate.

Infrared (IR) spectrometry studies were performed in a Shimadzu IR Prestige 21 spectrometer, measuring spectra of 64 scans at a spectral resolution of 4 cm^{-1}. A sample of 20 mg of Ni/Al$_2$O$_3$-HTC was placed into a Pike diffuse reflectance infrared Fourier transform spectroscopy (DRIFTS) sample cell. The catalyst was pre-treated at 500 °C under a flow of 10 mL·min^{-1} H$_2$ and 50 mL·min^{-1} argon (Ar) prior to measurements. The reaction was studied by flowing 10 mL·min^{-1} of CO$_2$ and 40 mL·min^{-1} of H$_2$ in 50 mL·min^{-1} of Ar, at atmospheric pressure and at several temperatures, with a 10 °C/min heating ramp. Each spectrum was baseline corrected with a background spectrum recorder at the same temperature under a flow of pure argon. Surface area and pore volume of the catalyst before and after reduction with H$_2$ were measured by N$_2$ adsorption-desorption isotherms with a Nova 1200e surface area analyzer from Quantachrome. Before analyses, the samples were pre-treated under vacuum at 300 °C for 3 h. The surface area was calculated through the multi-point BET method, and pore size distribution was calculated through the BJH method with the adsorption curves. Transmission electron microscopy (TEM) images were acquired using a JEOL JEM 2100 microscope, operating at 200 kV of acceleration voltage

with a LaB6 filament. The sample was dispersed in isopropanol with sonication, and dripped onto an ultrathin carbon film coated Cu grid. The histogram of nanoparticle size distribution was evaluated through these images by measuring 200 particles with ImageJ and fitting the histogram with a log-normal function. Origin 2019 software was used for data treatment and graphical illustrations of the reactions and characterization techniques.

4. Conclusions

The use of high pressure as tool to enhance the activity of a catalytic process for the production of methane from CO_2 hydrogenation was presented over a Ni/Al_2O_3-HTC catalyst. A selectivity of 100% for CH_4 was obtained over the range of temperatures studied of 350 to 450 °C at pressures of 20 to 80 bar. Therefore, the utilization of CO_2 for the production of methane, the main component of natural gas, has been demonstrated to be highly effective in the high-pressure catalytic process shown here. Thus, this is an efficient catalytic route to reducing CO_2 emissions with readily available non-noble metals with high production rates of 5.1 $L \cdot g_{cat}^{-1} \cdot h^{-1}$ of CH_4.

Supplementary Materials: The following supporting information can be downloaded at: https://www.mdpi.com/article/10.3390/methane3010004/s1, Figure S1: N_2 adsorption and desorption isotherm of as prepared Ni/Al_2O_3-HTC; Figure S2: N_2 adsorption and desorption isotherm of Ni/Al_2O_3-HTC reduced at 500 °C under H_2; Figure S3: BJH Pore size distribution performed on the adsorption isotherm of as prepared Ni/Al_2O_3-HTC; Figure S4: BJH Pore size distribution performed on the adsorption isotherm of Ni/Al_2O_3-HTC reduced at 500 °C under H_2; Figure S5: XPS of the O 1s region on Ni/Al_2O_3-HTC; Figure S6: TPD-CO_2 profile of Ni/Al_2O_3-HTC pre-reduced at 500 °C under H_2; Figure S7: Time on stream plot of the CO_2 methanation reaction over Ni/Al_2O_3-HTC. Reaction conditions: 200 mg of catalyst pre-reduced at 500 °C under H_2 for 1 h, T = 400 °C, p = 40 bar, GHSV = 30,000 $mL \cdot g_{cat}^{-1} \cdot h^{-1}$.

Author Contributions: Conceptualization, M.L.G., A.L.F. and P.V.; methodology, M.L.G., A.L.F., L.R.B. and R.R.; formal analysis, M.L.G. and L.R.B.; investigation, M.L.G., A.L.F. and L.R.B.; resources, P.V. and A.F.P.; writing—original draft preparation, M.L.G.; writing—review and editing, A.L.F., L.R.B., P.V., R.R. and A.F.P.; supervision, P.V. and A.F.P.; project administration, P.V. and A.F.P.; funding acquisition, P.V. and A.F.P. All authors have read and agreed to the published version of the manuscript.

Institutional Review Board Statement: Not applicable.

Informed Consent Statement: Not applicable.

Data Availability Statement: Data are contained within the article and Supplementary Materials.

Conflicts of Interest: The authors declare no conflicts of interest.

References

1. Yilmaz, H.Ü.; Kimbrough, S.O.; van Dinther, C.; Keles, D. Power-to-gas: Decarbonization of the European electricity system with synthetic methane. *Appl. Energy* **2022**, *323*, 119538. [CrossRef]
2. Genovese, M.; Schlüter, A.; Scionti, E.; Piraino, F.; Corigliano, O.; Fragiacomo, P. Power-to-hydrogen and hydrogen-to-X energy systems for the industry of the future in Europe. *Int. J. Hydrogen Energy* **2023**, *48*, 16545–16568. [CrossRef]
3. De Dokania, S.A.; Ramirez, A.; Gascon, J. Advances in the Design of Heterogeneous Catalysts and Thermocatalytic Processes for CO_2 Utilization. *ACS Catal.* **2020**, *10*, 14147–14185.
4. Nemmour, A.; Inayat, A.; Janajreh, I.; Ghenai, C. Green hydrogen-based E-fuels (E-methane, E-methanol, E-ammonia) to support clean energy transition: A literature review. *Int. J. Hydrogen Energy* **2023**, *48*, 29011–29033. [CrossRef]

5. Li, W.; Wang, H.; Jiang, X.; Zhu, J.; Liu, Z.; Guo, X.; Song, C. A short review of recent advances in CO_2 hydrogenation to hydrocarbons over heterogeneous catalysts. *RSC Adv.* **2018**, *8*, 7651–7669. [CrossRef]

6. Stangeland, K.; Kalai, D.; Li, H.; Yu, Z. CO_2 Methanation: The Effect of Catalysts and Reaction Conditions. In *Energy Procedia*; Elsevier Ltd.: Amsterdam, The Netherlands, 2017; pp. 2022–2027.

7. Lv, C.; Xu, L.; Chen, M.; Cui, Y.; Wen, X.; Li, Y.; Wu, C.E.; Yang, B.; Miao, Z.; Hu, X.; et al. Recent Progresses in Constructing the Highly Efficient Ni Based Catalysts with Advanced Low-Temperature Activity Toward CO_2 Methanation. *Front. Chem.* **2020**, *8*, 269. [CrossRef]

8. El-Salamony, R.A.; Acharya, K.; Al-Fatesh, A.S.; Osman, A.I.; Alreshaidan, S.B.; Kumar, N.S.; Ahmed, H.; Kumar, R. Enhanced direct methanation of CO_2 using Ni-based catalysts supported on ZrO_2, CeO_2-ZrO_2, and La_2O_3-ZrO_2: The effect of support material on the reducible NiO-interacted species and catalytic activity. *Mol. Catal.* **2023**, *547*, 113378. [CrossRef]

9. El-Salamony, R.A.; Al-Fatesh, A.S.; Acharya, K.; Abahussain, A.A.M.; Bagabas, A.; Kumar, N.S.; Ibrahim, A.A.; Khan, W.U.; Kumar, R. Carbon Dioxide Valorization into Methane Using Samarium Oxide-Supported Monometallic and Bimetallic Catalysts. *Catalysts* **2023**, *13*, 113. [CrossRef]

10. Garbarino, G.; Riani, P.; Magistri, L.; Busca, G. A study of the methanation of carbon dioxide on Ni/Al_2O_3 catalysts at atmospheric pressure. *Int. J. Hydrogen Energy* **2014**, *39*, 11557–11565. [CrossRef]

11. Zhang, Z.; Tian, Y.; Zhang, L.; Hu, S.; Xiang, J.; Wang, Y.; Xu, L.; Liu, Q.; Zhang, S.; Hu, X. Impacts of nickel loading on properties, catalytic behaviors of Ni/γ–Al2O3 catalysts and the reaction intermediates formed in methanation of CO_2. *Int. J. Hydrogen Energy* **2019**, *44*, 9291–9306. [CrossRef]

12. Zhang, G.; Liu, J.; Xu, Y.; Sun, Y. A review of CH_4 CO_2 reforming to synthesis gas over Ni-based catalysts in recent years (2010–2017). *Int. J. Hydrogen Energy* **2018**, *43*, 15030–15054. [CrossRef]

13. He, L.; Lin, Q.; Liu, Y.; Huang, Y. Unique catalysis of Ni-Al hydrotalcite derived catalyst in CO_2 methanation: Cooperative effect between Ni nanoparticles and a basic support. *J. Energy Chem.* **2014**, *23*, 587–592. [CrossRef]

14. Huynh, H.L.; Yu, Z. CO_2 Methanation on Hydrotalcite-Derived Catalysts and Structured Reactors: A Review. *Energy Technol.* **2020**, *8*, 1901475. [CrossRef]

15. Jia, C.; Gao, J.; Dai, Y.; Zhang, J.; Yang, Y.J. The thermodynamics analysis and experimental validation for complicated systems in CO2 hydrogenation process. *Energy Chem.* **2016**, *25*, 1027–1037. [CrossRef]

16. Jürgensen, L.; Ehimen, E.A.; Born, J.; Holm-Nielsen, J.B. Dynamic biogas upgrading based on the Sabatier process: Thermodynamic and dynamic process simulation. *Bioresour. Technol.* **2015**, *178*, 323–329. [CrossRef]

17. Mutz, B.; Belimov, M.; Wang, W.; Sprenger, P.; Serrer, M.A.; Wang, D.; Pfeifer, P.; Kleist, W.; Grunwaldt, J.D. Potential of an alumina-supported Ni3Fe catalyst in the methanation of CO_2: Impact of alloy formation on activity and stability. *ACS Catal.* **2017**, *7*, 6802–6814. [CrossRef]

18. Abate, S.; Barbera, K.; Giglio, E.; Deorsola, F.; Bensaid, S.; Perathoner, S.; Pirone, R.; Centi, G. Synthesis, Characterization, and Activity Pattern of Ni–Al Hydrotalcite Catalysts in CO_2 Methanation. *Ind. Eng. Chem. Res.* **2016**, *55*, 8299–8308. [CrossRef]

19. Xu, Y.; Du, X.; Shi, L.; Chen, T.; Wan, H.; Wang, P.; Wei, S.; Yao, B.; Zhu, J.; Song, M. Improved performance of Ni/Al_2O_3 catalyst deriving from the hydrotalcite precursor synthesized on Al_2O_3 support for dry re-forming of methane. *Int. J. Hydrogen Energy* **2021**, *46*, 14301–14310. [CrossRef]

20. Doebelin, N.; Kleeberg, R. Profex: A graphical user interface for the Rietveld refinement program BGMN. *J. Appl. Crystallogr.* **2015**, *48*, 1573–1580. [CrossRef]

21. Yi, H.; Xue, Q.; Lu, S.; Wu, J.; Wang, Y.; Luo, G. Effect of pore structure on Ni/Al_2O_3 microsphere catalysts for enhanced CO_2 methanation. *Fuel* **2022**, *315*, 123262. [CrossRef]

22. Pieta, I.S.; Lewalska-Graczyk, A.; Kowalik, P.; Antoniak-Jurak, K.; Krysa, M.; Sroka-Bartnicka, A.; Gajek, A.; Lisowski, W.; Mrdenovic, D.; Pieta, P.; et al. CO_2 Hydrogenation to Methane over Ni-Catalysts: The Effect of Support and Vanadia Promoting. *Catalysts* **2021**, *11*, 433. [CrossRef]

23. Gao, H.-B.; Qiu, L.-L.; Wu, F.-P.; Xiao, J.; Zhao, Y.-P.; Liang, J.; Bai, Y.-H.; Liu, F.-J.; Cao, J.-P. Highly efficient catalytic hydrogenolysis of lignin model compounds over hydrotalcite-derived Ni/Al_2O_3 catalysts. *Fuel* **2023**, *337*, 127196. [CrossRef]

24. Jin, B.; Li, S.; Liang, X. Enhanced activity and stability of MgO-promoted Ni/Al_2O_3 catalyst for dry reforming of methane: Role of MgO. *Fuel* **2021**, *284*, 119082. [CrossRef]

25. Chen, J.; Ma, Q.; Rufford, T.E.; Li, Y.; Zhu, Z. Influence of calcination temperatures of Feitknecht compound precursor on the structure of Ni–Al_2O_3 catalyst and the corresponding catalytic activity in methane decomposition to hydrogen and carbon nanofibers. *Appl. Catal. A Gen.* **2009**, *362*, 1–7. [CrossRef]

26. NIST X-ray Photoelectron Spectroscopy Database. *NIST Standard Reference Database Number 20*; National Institute of Standards and Technology: Gaithersburg, MD, USA, 2000; p. 20899. [CrossRef]

27. Crist, B.V. *Monochromatic XPS Spectra Commercially Pure Binary Oxides*; XPS International, LLC: Salem, OR, USA, 2019.

28. Liu, Z.; Chu, B.; Zhai, X.; Jin, Y.; Cheng, Y. Total methanation of syngas to synthetic natural gas over Ni catalyst in a micro-channel reactor. *Fuel* **2012**, *95*, 599–605. [CrossRef]

29. Hashimoto, N.; Mori, K.; Asahara, K.; Shibata, S.; Jida, H.; Kuwahara, Y.; Yamashita, H. How the Morphology of NiO_x-Decorated CeO_2 Nanostructures Affects Catalytic Properties in CO_2 Methanation. *Langmuir* **2021**, *37*, 5376–5384. [CrossRef]

30. Cárdenas-Arenas, A.; Cortés, H.S.; Bailón-García, E.; Davó-Quiñonero, A.; Lozano-Castelló, D.; Bueno-López, A. Active, selective and stable NiO-CeO_2 nanoparticles for CO_2 methanation. *Fuel Proces. Technol.* **2021**, *212*, 106637. [CrossRef]

31. Atzori, L.; Cutrufello, M.G.; Meloni, D.; Cannas, C.; Gazzoli, D.; Monaci, R.; Sini, M.F.; Rombi, E. Highly active NiO-CeO$_2$ catalysts for synthetic natural gas production by CO$_2$ methanation. *Catal. Today* **2018**, *299*, 183–192. [CrossRef]

32. Ramos, R.; Peixoto, A.F.; Arias-Serrano, B.I.; Soares, O.S.G.P.; Pereira, M.F.R.; Kubička, D.; Freire, C. Catalytic Transfer Hydrogenation of Furfural over Co$_3$O$_4$–Al$_2$O$_3$ Hydrotalcite-derived Catalyst. *ChemCatChem* **2020**, *12*, 1467–1475. [CrossRef]

33. Wierzbicki, D.; Motak, M.; Grzybek, T.; Gálvez, M.E.; Da Costa, P. The influence of lanthanum incorporation method on the performance of nickel-containing hydrotalcite-derived catalysts in CO$_2$ methanation reaction. *Catal. Today* **2018**, *307*, 205–211. [CrossRef]

34. Han, F.; Liu, Q.; Li, D.; Ouyang, J. An emerging and high-performance sepiolite-supported Ni catalyst for low-temperature CO$_2$ methanation: The critical role of hydroxyl groups. *J. Environ. Chem. Eng.* **2023**, *11*, 110331. [CrossRef]

35. Cárdenas-Arenas, A.; Quindimil, A.; Davó-Quiñonero, A.; Bailón-García, E.; Lozano-Castelló, D.; De-La-Torre, U.; Pereda-Ayo, B.; González-Marcos, J.A.; González-Velasco, J.R.; Bueno-López, A. Isotopic and in situ DRIFTS study of the CO$_2$ methanation mechanism using Ni/CeO$_2$ and Ni/Al$_2$O$_3$ catalysts. *Appl. Catal. B* **2020**, *265*, 118538. [CrossRef]